DR. 2983

UCRL-52680

A REGIONAL WIND-FIELD STUDY IN COMPLEX TERRAIN DURING SUMMER SEA-BREEZE CONDITIONS

W.M. Porch
P.A. Volker
K.R. Peterson
R.L. Weichel
C. Sherman

March 5, 1979

Work performed under the auspices of the U.S. Department of Energy by the UCLLL under contract number W-7405-ENG-48.

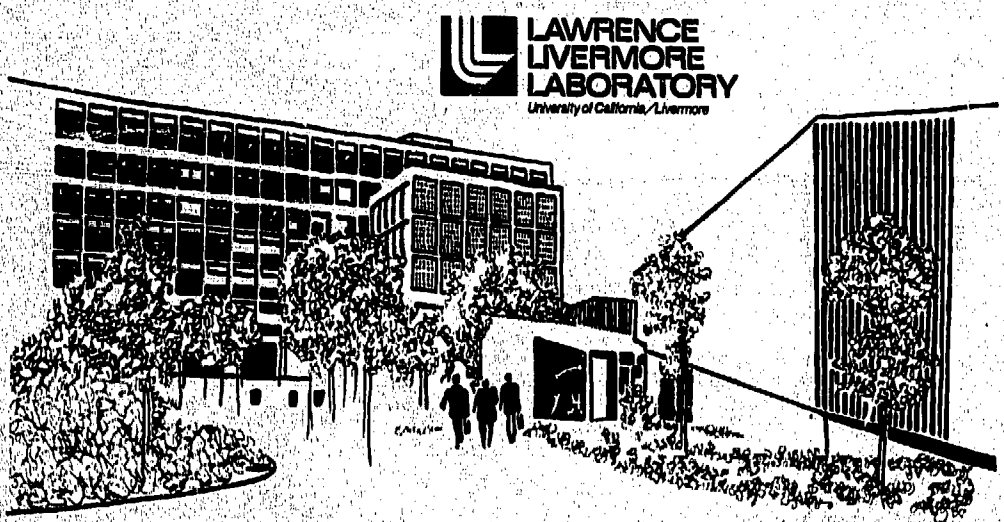

Distribution Category
UC-11

LAWRENCE LIVERMORE LABORATORY
University of California/Livermore, California/94550

UCRL-52680

A REGIONAL WIND-FIELD STUDY IN COMPLEX TERRAIN DURING SUMMER SEA-BREEZE CONDITIONS

W.M. Porch
P.A. Volker
K.R. Peterson
R.L. Weichel
C. Sherman

MS date: March 5, 1979

CONTENTS

A REGIONAL WIND-FIELD STUDY IN COMPLEX TERRAIN DURING SUMMER SEA-BREEZE CONDITIONS

ABSTRACT

A regional-scale data base, consisting of wind and temperature data for June and July of 1977, was developed for the greater San Francisco Bay Area and eastward to the Central Valley. Continuous meteorological measurements were made in the area of a windy pass (Patterson Pass) 3 km east of Lawrence Livermore Laboratory. This area was chosen because of its complex terrain and importance as a downwind topographic feature affecting the dispersal of possible accidental atmospheric releases from the Laboratory and as an area of high wind-energy potential. The results of this study provided the following:

1. A data base, including over 50 stations for use in numerical wind-field regional-scale-model validation.
2. Characterization of summer sea breeze oscillations of ~6 and 12 days. This analysis is useful in calculating wind-power persistence and in understanding summer sea-breeze mechanisms in the Bay Area.
3. Successful application of an optical space-averaging wind sensor over a 1-km path across a pass to provide long-path averaged data more suitable for regional, numerical wind-field models with kilometre-size grid elements.

INTRODUCTION

The recent development of large computers has enabled significant improvement in the quality of regional-scale, numerical wind-field models. At Lawrence Livermore Laboratory (LLL), these models have been used to assess the downwind transport of pollutants and to find areas of high wind-energy potential. In recent years, we have made a concentrated effort to use and validate these models in areas of complex terrain. This task was not simple because meteorological measurements are rarely made in complex terrain; nearly all routine wind observations are made at airports or within population centers. In addition, the output of our numerical wind models yield winds averaged over grid cells on the order of a kilometre.[1] Instrument exposure problems in complex terrain for conventional anemometers are such that one station can rarely represent the average wind over a distance of 1 km. Another problem associated with establishing a high-quality data base on a regional scale is that of data density. To characterize a regional-scale wind field, input data points must be sufficiently dense to define the terrain-induced wind regimes.

We designed and executed an experiment to develop a data base for numerical wind-field validation. Two elements were involved in the experiment. First, we conducted a concentrated measurement program at Patterson Pass, an area of complex terrain 3 km east of LLL. We chose this area because it has a high wind-energy potential and because it is a topographic feature that strongly influences the downwind dispersal of possible accidental atmospheric releases from LLL. Second, while data were collected at Patterson Pass during June and July, 1977, data were also being collected from more than fifty locations throughout the San Francisco Bay Area and Central Valley. In addition radiosonde data from Oakland were collected twice daily and acoustic-sounder data were recorded continuously at Livermore. Wind and sea-surface temperature data for two ocean locations off the west coast were obtained from the Fleet Numerical Weather Service at Monterey, California, and incorporated into the data base.

The measurement program at Patterson Pass involved wind measurements with a conventional cup anemometer at a height of 5 m over a level area

on the south side of Patterson Pass, and optical (both laser and white-light) wind-speed measurements of the average wind through the Pass, using a 1-km optical path. Lawrence, et al.,[2] and Ochs, et al.,[3] describe these techniques in detail. Subsequent analysis of these data showed a correlation coefficient of 0.91 between the long-path optically derived winds and the winds measured with the conventional cup anemometer; however, on many occasions the values differed by many metres per second. These results indicate that the optical anemometers were operating satisfactorily and that, as expected, a single, conventional wind measurement cannot represent short-term average winds over a kilometre in areas of complex terrain.

Combining the data from Patterson Pass with wind data from the other stations in the region, we developed a data matrix which we statistically analyzed for application to numerical wind-field validation. True validation of a wind-field model requires the comparison of calculations with and without the presence of data from selected stations to compare predicted and measured winds in the vicinity of the stations. Choosing the stations to be reserved for comparison is difficult because few of the stations in the data base are actually in areas of complex terrain. However, many stations in level terrain still provide important information about the flow field in the complex terrain regions. Other stations contribute little important information because their data provide either duplicate information to another station nearby or random data that are useless in wind-field estimates because of poor exposure or other instrument problems.

We statistically analyzed the data matrix to choose representative stations for use in the validation study. The complete data matrix was analyzed, using multiple linear regression, to determine which stations significantly contribute to predicting winds at Patterson Pass for the two-month period. The use of multiple linear regression ensures two things:

1. Elimination of stations with poor data due to instrument errors, location and exposure problems, or redundant data.

2. Development of a rational scheme for the selective elimination of input data to computer models for their validation.

The second item is achieved by varying the statistical F-test in the linear regression. Not all the stations chosen by this procedure were close to Patterson Pass. One station close to the pass and several others, representative of the various flow regimes of the region, were selected.

The data period chosen coincided with the summer sea-breeze period in this region.[4] Therefore, the data were found useful not only as a base for model validation but also as a resource for understanding the characteristics of the sea breeze in the region. Power spectra analyses and correlations of ocean data and air temperatures with winds in the region proved useful in understanding the sea breeze. Spectral analyses showed a recurrent 6- and ~12-day peak in wind speeds and air temperatures; they also showed negative correlation between air temperatures and winds over land areas, as well as a time lag of many days between changes in ocean wind and sea-surface temperatures and Central Valley temperatures. These results provide useful supplements to previous sea breeze studies.[5-8]

The results described in the following sections are divided into two parts. The first part emphasizes the measurement program at Patterson Pass. The second part relates the Patterson Pass data to the other data from the region. It presents the results of the statistical analysis applied to the summer sea breeze and the results of the regression analysis used to choose stations for model validation. The results of that model validation will be presented in a subsequent report.

RESULTS OF MEASUREMENT PROGRAM IN COMPLEX TERRAIN

SITE DESCRIPTION

The measurement program at Patterson Pass was conducted during June and July, 1977, using the following instruments:

- A space-averaging laser anemometer (Campbell Scientific Model #CA-9) over a 1.03-km path across the Pass; the path was oriented 20° west of true north and nearly perpendicular to the lowest part of the Pass.

• A white-light optical anemometer provided by the National Oceanic and Atmospheric Administration Wave Propagation Laboratory (NOAA-WPL) oriented along the same path in the opposite direction.

• A mechanical weather station (Meteorological Research Incorporated Model No. 1071) located at the south end of the light path.

Figure 1 is a photograph of the experimental arrangement. The optical anemometers were housed in instrument shelters to protect them from the elements and wind vibration. The white-light transmitter can be seen at the north end of the light path. A laser was simultaneously transmitting in the opposite direction and being received at an instrument shelter near the white light. Figure 2 shows the terrain relief under the light path. The transmitter and receiver were 526 and 560 m, respectively, above sea level, with the lowest section of the Pass at 464 m. The space-averaging laser anemometer was run continuously through the two-month period, whereas the white-light system was run at selected intervals for comparison. All data were collected on strip-chart recorders. Figure 3 shows the laser anemometer reading for a windy period during July 4. The wind speeds on the chart refer to the average wind component normal to the optical path, weighted toward the center of the Pass.[2]

OPTICAL ANEMOMETER COMPARISON

Figure 4 compares the readings of the laser system with the white-light system along the same path for July 13. The white-light system has a similar, but somewhat more peaked, weighting function.[3] These data represent the westward component of the wind normal to the light path. The cross-path winds from the space-averaging laser anemometer and the wind speed and direction from the mechanical weather station were averaged over 30-min periods, digitized, and compared. The 30-min interval was based on a comparison of similar data taken at a rate of once per second at Honolulu, Hawaii.[9] These Hawaiian data indicated that the spatial averaging properties of the optical anemometer show a temporal averaging effect over data periods $\lesssim$ 10 min along a 1-km path. This effect is represented through a change in slope of the

Fig. 1. Photograph of experimental setup in complex terrain looking north across Patterson Pass. A cup-vane-anemometer and optical-anemometer receiving station is in the foreground; a light source and duplicate laser optical-anemometer receiving station is in the background.

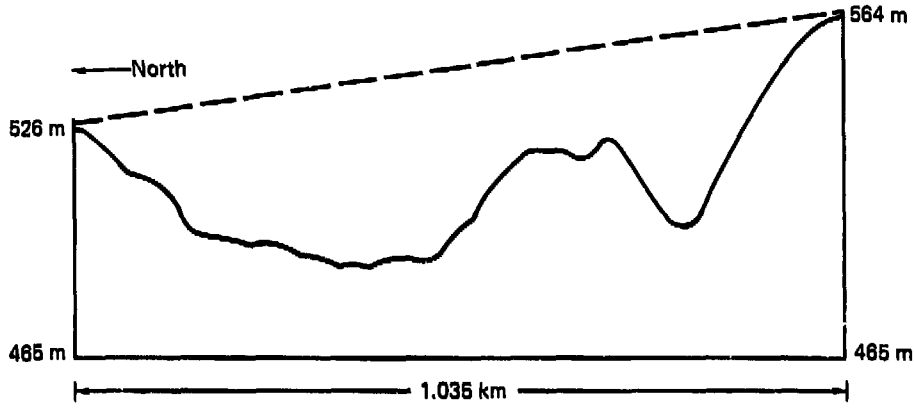

Fig. 2. Relief topography of Patterson Pass beneath laser beam.

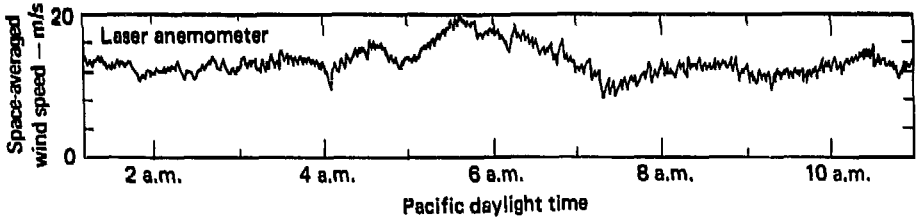

Fig. 3. An example of strip chart data from laser space-averaging optical anemometer during a windy night, July 4, 1977.

standard deviation of the wind-speed component normal to the light path at ~10 min for a cup-anemometer system and only at ~1 min for the optical-anemometer system. Figure 5 shows time plots and scatter plots of 30-min-average cross winds from the laser optical anemometer and the component of the wind speed perpendicular to the light path derived from cup and vane system at the south end of the path. Daytime (1000-2200 PDT) and nighttime data are shown separately in the scatter plots. The total data correlation coefficient was 0.91 with the regression equation:

> Laser optical-anemometer speed = 1.62 + 0.94 × (cross-beam wind component from cup and vane anemometers).

Splitting the data into (1) day and night or (2) wind speeds less than or greater than 8 m/s did not significantly improve that correlation coefficient.

The higher value associated with the optical-anemometer speed (1.62 m/s) over the cup-vane system probably results from the greater height of the light beam above topography. The average height of the light path above terrain was 38 m; the cup-vane anemometer height was 5.5 m. Based on this height difference, the power-law wind-profile equation has an exponent (p) of 0.12, which is within the expected range for a windy area. This ratio was determined from:

$$\overline{OA}\ (\text{m/s}) = \left(\frac{38\text{m}}{5.5\text{m}}\right)^{p} \overline{WS}_{\perp}\ (\text{m/s})$$

where $\overline{OA}$ = average speed from optical anemometer (7.9 m/s)

$\overline{WS}_{\perp}$ = average speed perpendicular to light path, derived from the weather station (6.5 m/s).

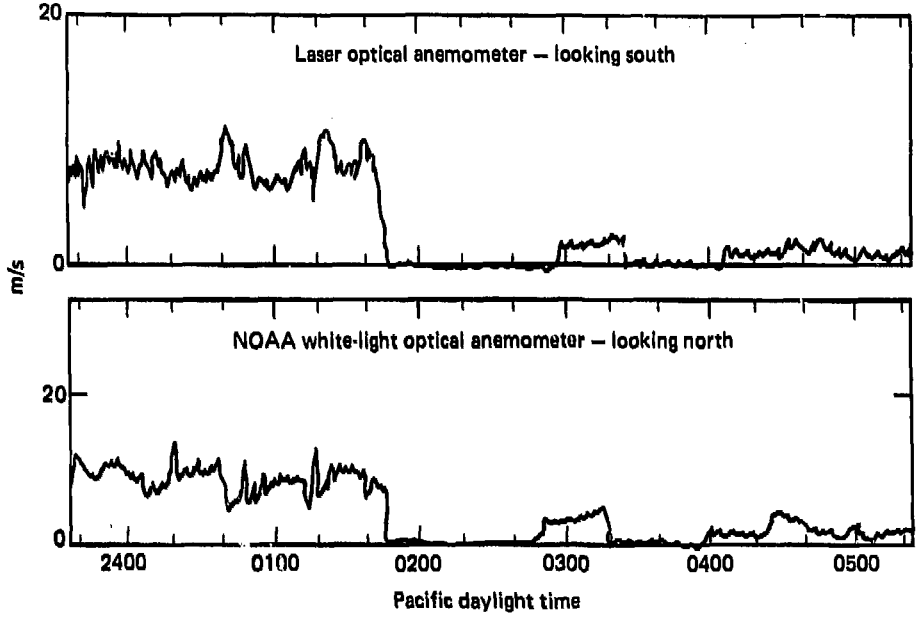

Fig. 4. A comparison of the laser optical anemometer and a white-light (saturation resistant) optical anemometer looking in opposite directions along the same path in complex terrain (Patterson Pass). (Zero value in this case implies a wind direction along the beam or eastward.)

Besides height, differences in instrument exposure and types of measurements, i.e., point measurement or spatially averaged measurement, were also factors affecting this ratio.

Thirty-minute-average data were also collected from a 40-m tower at LLL and a 36-m tower at Livermore Site 300. These stations are located 7.5 km west and 9.6 km south, respectively, of the measurement stations at Patterson Pass. Both are permanent stations maintained by the Laboratory; relationships between the data from these stations and the wind speeds at Patterson Pass may be useful in the future to predict summer winds at the Pass, where a station does not normally exist. These relationships are summarized in Table 1, which lists the parameters involved as well as the average values, correlations, and regression formulas for these parameters.

TEMPORAL COMPARISON BETWEEN POINT AND OPTICAL ANEMOMETER

We applied spectral analysis to these 30-min-averaged data to better understand the cyclic behavior of summer sea-breeze winds. Figure 6 shows the normalized power spectral density as a function of time in days for (a) the weather station wind speeds, (b) the optical-anemometer cross-path speeds, (c) the weather-station-derived cross-path speeds, (d) the wind speeds at Site 300, and (e) the wind speeds at the 40-m tower at LLL. The spectra for each of these data sources show a strong diurnal peak, as well as many similarities at low frequencies. Comparison of the power spectra for the optical anemometer with the cross-wind component derived from the weather station shows a greater

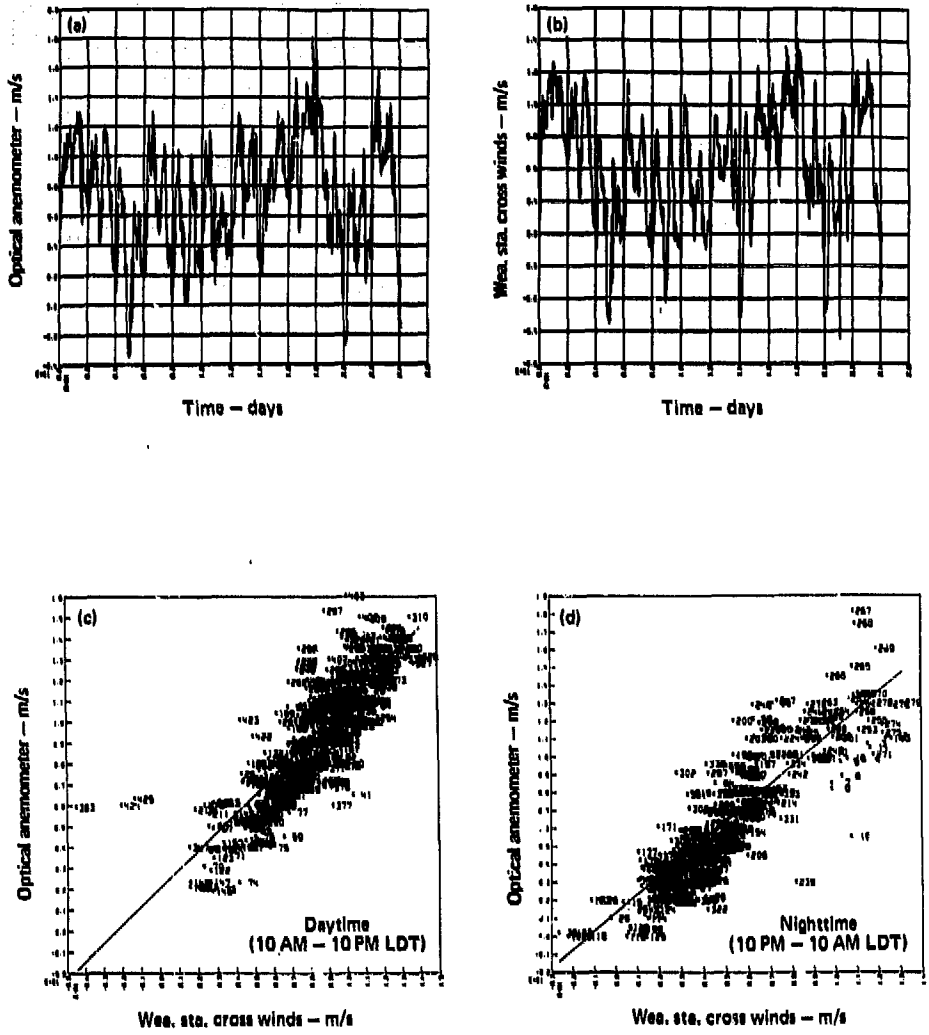

Fig. 5. A comparison of simultaneous laser space-averaging optical-anemometer data and the perpendicular component of the winds measured at the south end of the light path.

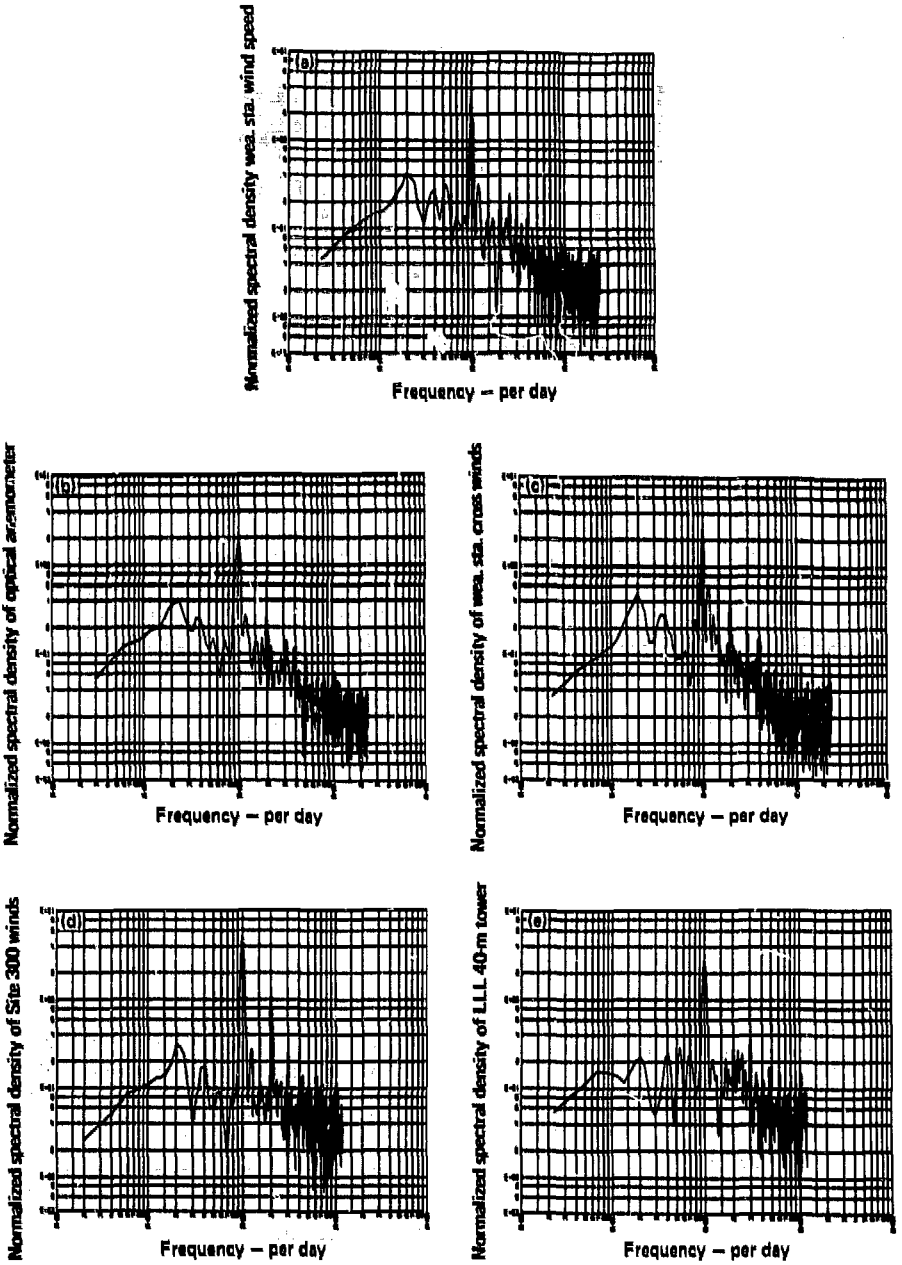

Fig. 6. The normalized power, spectral density as a function of frequency in (per day) for the weather station wind speeds (a), the laser optical-anemometer cross-path speeds (b), the weather-station-derived cross path speeds (c), the wind speeds at Site 300 (d), and the wind speeds at the 40-m tower at LLL (e).

Table 1. Statistical relationships between the wind speeds measured at Patterson Pass at 5.5 m by a cup anemometer and wind speeds at L.L.L. and Site 300 at heights of 40 and 36 m, respectively.

Wind station location	Standard deviation	Average value	Correlation	Regression equation
At weather station (Patterson Pass)	3.5 m/s	7.9 m/s (total) 8.5 m/s (day) 7.0 m/s (night)	0.64 (total) 0.67 (day) 0.63 (night)	A = 4.93 + 0.41 B A = 4.88 + 0.38 B A = 5.17 + 0.45 B
At L.L.L. 40-m tower	5.1 m/s	6.6 m/s (total) 8.6 m/s (day) 5.3 m/s (night)		
At weather station (Patterson Pass)	3.5 m/s	7.86 m/s	0.66 (total) 0.67 (day) 0.67 (night)	A = 4.12 + 0.51 B A = 4.21 + 0.53 B A = 3.86 + 0.49 B
At Site 300	3.8 m/s	7.85 m/s (total) 8.4 m/s (day) 7.2 m/s (night)		

difference and spread in the spectra for the weather station at frequencies less than once per day. This again demonstrates the problem of using a single conventional measurement in areas of complex terrain to derive average winds over a distance suitable for model validation. The differences in the lower frequency spectra between the weather station wind speeds and their component perpendicular to the light path between once every 5 days and once each day are the result of spectral energy in the once-per-two-day variation in the normal component of the wind direction.

This variation is not present in the wind-speed spectra. However, the wind-direction normal component, as well as all the other spectra, demonstrates a strong one-per-five-day oscillation (frequency = 0.2 per day). Because these data were taken at the maximum of the summer sea breeze and the intensity of the sea breeze is known to vary periodically, these spectra represent a quantification of this period. Indirect evidence, through solar insolation studies, seems to indicate a similar period for fog duration.[10] Subsequent analysis of regional wind data with a maximum-entropy spectral technique also reveals an even lower oscillation at about once every 12-16 days. Taken together with other data described in the next section of this report, these oscillations can be useful in understanding the mechanisms of the summer sea breeze.

Closer examination of the higher-frequency end of the spectra in Fig. 6 reveals a more subtle difference between spatially averaged winds and point winds. All the point-wind spectra show a tendency to increase, whereas the optical-anemometer spectra do not. This is even more apparent in Fig. 7, which shows the power spectra of the cosine of the wind direction normal to the laser optical path at (a) Patterson Pass, (b) Site 300, and (c) Livermore. The point-measurement spectra begin to rise at an even lower frequency (about once every four hours). Apparently, this is the result of an extended spectral gap during unstable conditions close to the ground in complex terrain.[11] Because of the longer wavelength of eddies affecting the spatially averaged winds, this spectral gap and the peak in the turbulent energy spectrum are suppressed. This implies that, at Patterson Pass, data from a single station must be averaged over a 2-h period to produce winds that vary similarly in speed and direction to 1-km spatially averaged winds.

COMBINATION OF COMPLEX TERRAIN DATA WITH REGIONAL METEOROLOGICAL DATA

DATA SOURCES

While the field measurement program was being conducted at Patterson Pass, data were being collected at meteorological stations in the San Francisco Area and Central Valley. Table 2 identifies

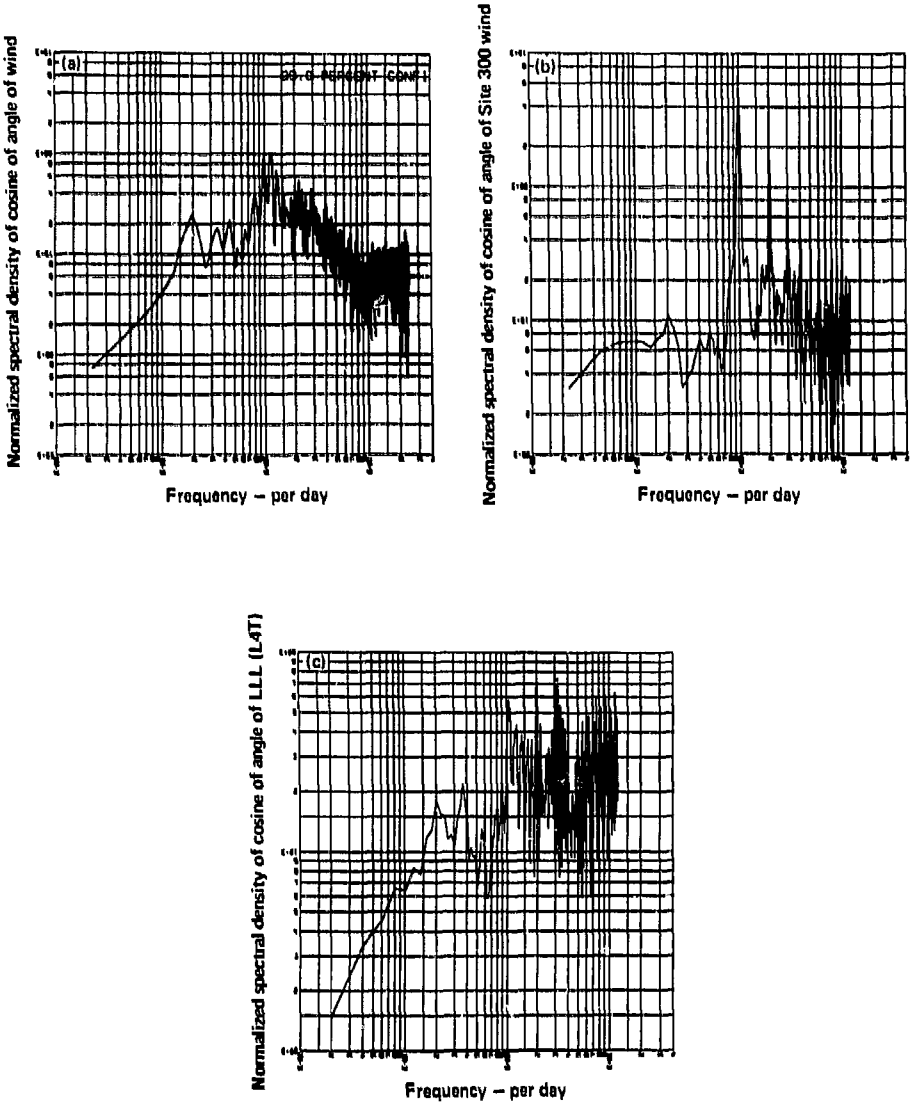

Fig. 7. Normalized power spectra for the cosine of the wind direction away from the laser optical path at (a) Patterson Pass, (b) Site 300, and (c) Livermore.

Table 2. Summary of regional data stations and their locations.

Station identification	UTM coordinates, km		Distance from Patterson Pass, km	Height above terrain, m
	North	East		
1. MRI Patterson Pass	4171.1	621.2	0.0	5.5
2. L4T L.L.L. Tower	4172.3	613.8	7.5	40.0
3. LLH Site 300	4168.2	630.4	9.6	36.0
4. DLL BAAPCD Livermore	4172.2	608.2	13.0	13.06
5. QBV QB Vallecitos	4160.0	605.0	19.6	13.7
6. CPH Pleasanton	4168.2	597.8	23.6	6.1
7. CFR C Fremont	4158.3	590.9	32.9	6.1
8. DFR D Fremont	4154.6	591.8	33.7	6.1
9. POA Oakley	4205.0	611.0	35.4	10.0
10. PBI Bethal Island	4209.0	621.0	37.9	10.0
11. SCU Stockton WSD	4195.4	653.8	40.7	6.1
12. PSI Sherman Island	4211.0	612.0	40.9	10.0
13. CST Stockton Cal Trans	4202.0	650.0	42.2	10.0
14. CWC Walnut Creek	4191.9	584.1	42.5	6.1
15. DSJ San Jose	4133.0	598.5	44.3	6.1
16. CSL San Leandro	4173.8	577.0	44.3	6.1
17. DPT Pittsburg Cal Trans	4209.4	597.3	45.1	6.1
18. DCO Concord	4199.3	585.7	45.3	6.1
19. EQP Pittsburg PGE	4210.2	596.7	46.1	6.1
20. NUQ Moffett Field	4141.2	584.1	47.6	6.1
21. DSY Sunnyvale	4136.7	585.9	49.3	6.1
22. OAK Oakland WSO	4176.2	570.4	51.0	6.1
23. CMH Morgan Hill	4118.1	619.9	53.0	6.1
24. DRC Redwood City	4148.5	570.5	55.5	6.1
25. HGZ Alameda NAS	4181.7	560.1	62.0	6.1
26. DBE Benicia	4211.8	574.3	62.1	6.1
27. CRT Crockett	4211.0	571.0	64.1	6.1
28. CBM Berkeley Marina	4191.2	560.0	64.4	6.1
29. DBU Burlingame	4159.1	557.8	64.5	6.1
30. CKE Keyes	4153.0	685.0	66.3	10.0
31. SFO San Francisco WSO	4163.2	554.4	67.3	6.1
32. SFE SFO Ellis St.	4182.0	552.5	69.6	6.1
33. SUU Travis AFB	4235.5	593.2	70.2	14.0
34. SF2 SFO 23rd Street	4181.8	551.1	70.9	6.1
35. DRM Richmond	4200.4	556.6	70.9	6.1
36. DVA Vallejo	4217.4	567.1	71.2	6.1
37. CGB Golden Gate Bridge	4185.0	550.0	72.5	113.0
38. DGL Gilroy	4096.8	627.2	74.5	6.1
39. DPA Pacifica	4163.0	547.0	74.6	6.1
40. CMD Menlo Pk (Dum. Brdg.)	4146.3	550.1	75.3	6.1
41. DSR San Rafael	4202.7	542.3	85.0	6.1
42. DNA Napa	4240.7	561.6	91.6	6.1
43. SAC Sacramento (EvAP)	4263.6	631.1	93.0	6.1
44. EGL Moss Landing	4074.1	608.7	97.8	76.2
45. MHR Mather AFB	4268.6	647.8	101.1	5.0
46. MCC McClellan AFB	4280.6	638.9	110.9	5.0
47. SNS Salinas WSO	4058.2	625.0	113.0	6.1
48. DSA Santa Rosa	4254.7	525.1	127.4	6.1
49. BAB Beale AFB	4332.1	635.3	161.6	6.0

these stations, gives their Universal Transverse Mercator (UTM) coordinates and wind-sensor height above terrain. Most of the meteorological stations provide air temperature as well as wind speed and direction. Data were also collected from the Fleet Numerical Weather Center in Monterey for ocean winds and sea-surface temperatures at 37.8 N and 123.0 W (about 10 km west of San Francisco) and 36.6 N and 122.4 W (about 10 km west of Monterey). These data were collected hourly; however, the comparisons and analyses that follow concentrate on two selected hours.

The first hour began at 2300 GMT (23Z or 1600 PDT) during the peak of sea-breeze intensity at Patterson Pass; the other hour began at 1100 GMT (11Z or 0400 PDT) at the typical sea-breeze minimum. Figures 8-12 show sample time plots taken from the stations listed in Table 2 and the ocean locations at 2300 GMT and 1100 GMT (0000 GMT or 0Z and 1200 GMT or 12Z for the ocean locations). These plots were derived from original data points and smoothed by a Whitacker-Henderson Type A formula[12] with a smoothing parameter of 0.2 for Figs. 8-11 to emphasize the long term cycles and 2.0 for Fig. 12 to show the long term trend. Figures 8 and 10 show the daily fluctuation of wind speed recorded at the stations listed in Table 2 at 2300 GMT or 1100 GMT, respectively, with ocean data off the coast of San Francisco [Fig. 8 (l)] . Figures 9 and 11 show analogous data for sample stations that reported air temperature at 2300 GMT and 1100 GMT, respectively. Also included in these figures are plots of the air temperature differences between San Francisco/Oakland and Sacramento/Stockton (see Figs. 9 and 11 (e), (f), (i), (k), and (l)) and sea-surface temperatures for the June and July data period off the coast of San Francisco, (Fig.9(g) and 11(g)) and the extended period (May-Aug.) off the coast of Monterey (Fig.9(k), as well as the ocean winds off the coast of Monterey (Fig. 9(j) and 11(j)).

Figure 12 shows the long term trends of selected data from the previous figures. Parts (i) and (j) of Fig. 12 show that the ocean winds peaked during the June-July data period while the ocean temperatures continued to increase. Parts (a), (b), (c) and (d) of Fig. 12 show that, though daytime winds continued to increase at Patterson Pass and Site 300, winds had a downward trend. The other data showed little or no trends.

DATA ANALYSIS USING TIME-LAGGED CORRELATION

A time-lagged correlation analysis was performed on the data shown in Figs. 8-12 and on other wind and temperature data from the region. The results of this analysis appear in Table 3 in the form of a correlation matrix with the time lag to maximum correlation shown in parentheses. A summary of the results of this correlation matrix follows:

1. Low and variable correlations exist between the ocean winds and sea surface temperatures and wind speeds throughout the Bay Area and Central Valley.

2. Higher correlations exist between air temperatures at the land stations and the ocean temperature and wind speeds.

3. Negative correlations exist between the air temperature data for the region and sea-surface temperatures.

4. Positive correlations exist between regional air temperatures and sea surface winds during the day; negative correlations exist at night.

5. Time lags of 1-3 days occur for maximum correlation with air temperatures in the region (increasing for stations as a function of their distance east from the coast) and sea-surface temperatures and wind speeds.

6. The temperature differences between the Central Valley and the coast correlate less with the ocean temperatures and wind speeds than the air temperatures alone in the Central Valley, implying that the differences are dominated by the temperatures in the valley.

7. Slightly higher correlations exist between the regional temperatures and the ocean temperatures and wind speeds off the coast of Monterey than off the coast of San Francisco.

8. The expected high negative correlation exists between regional air temperatures and sea-breeze wind speeds measured at Patterson Pass.

SPECTRAL ANALYSIS OF REGIONAL DATA

Power spectral analysis was also applied to these data. However, only 55 data points are available for each data set, too few for conventional spectral analysis techniques. In the past few years,

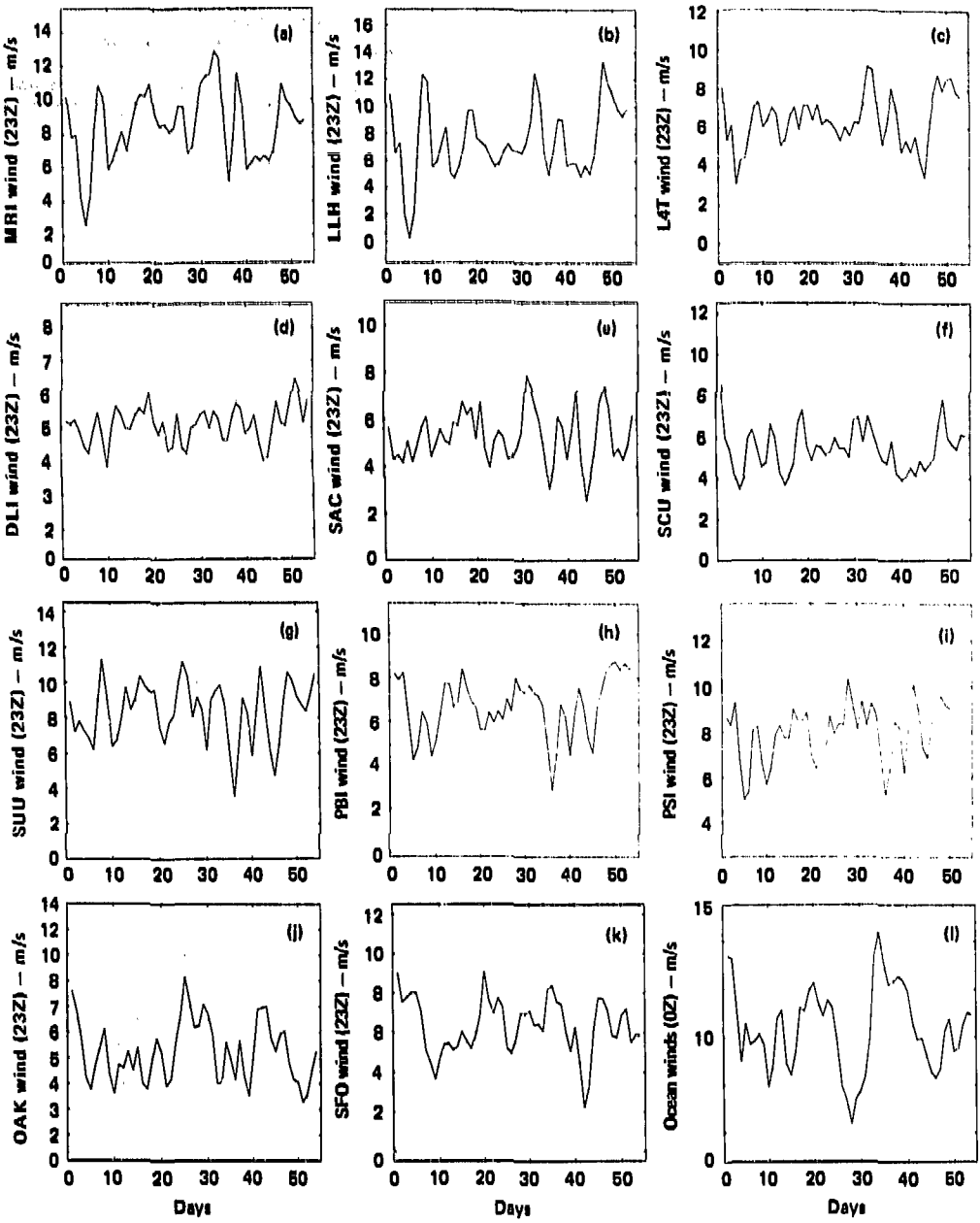

Fig. 8. Regional wind data at 2300 GMT or 23Z (1600 PDT) and 0Z for ocean data.

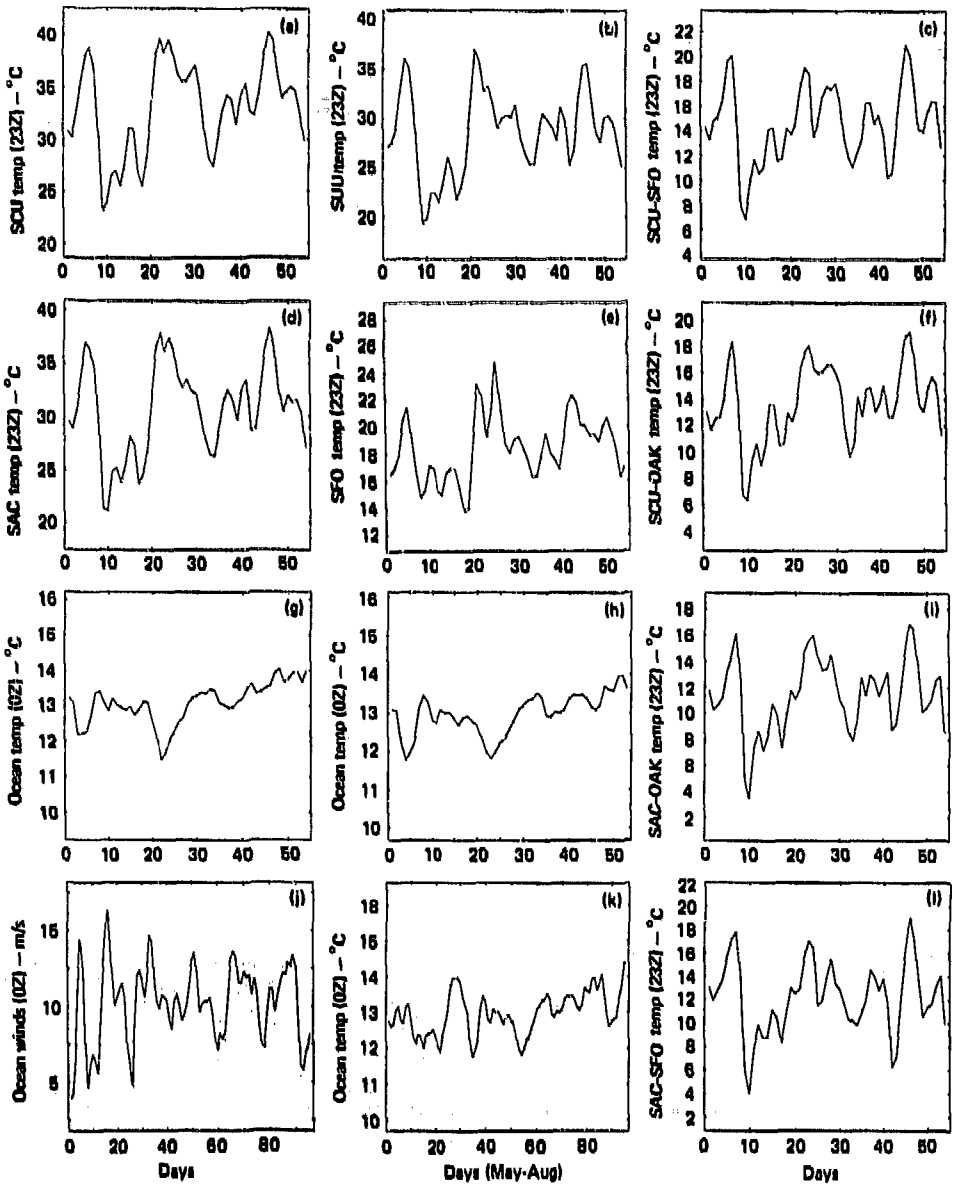

Fig. 9. Regional temperature and temperature-difference data at 23Z with ocean parameter data at 0Z.

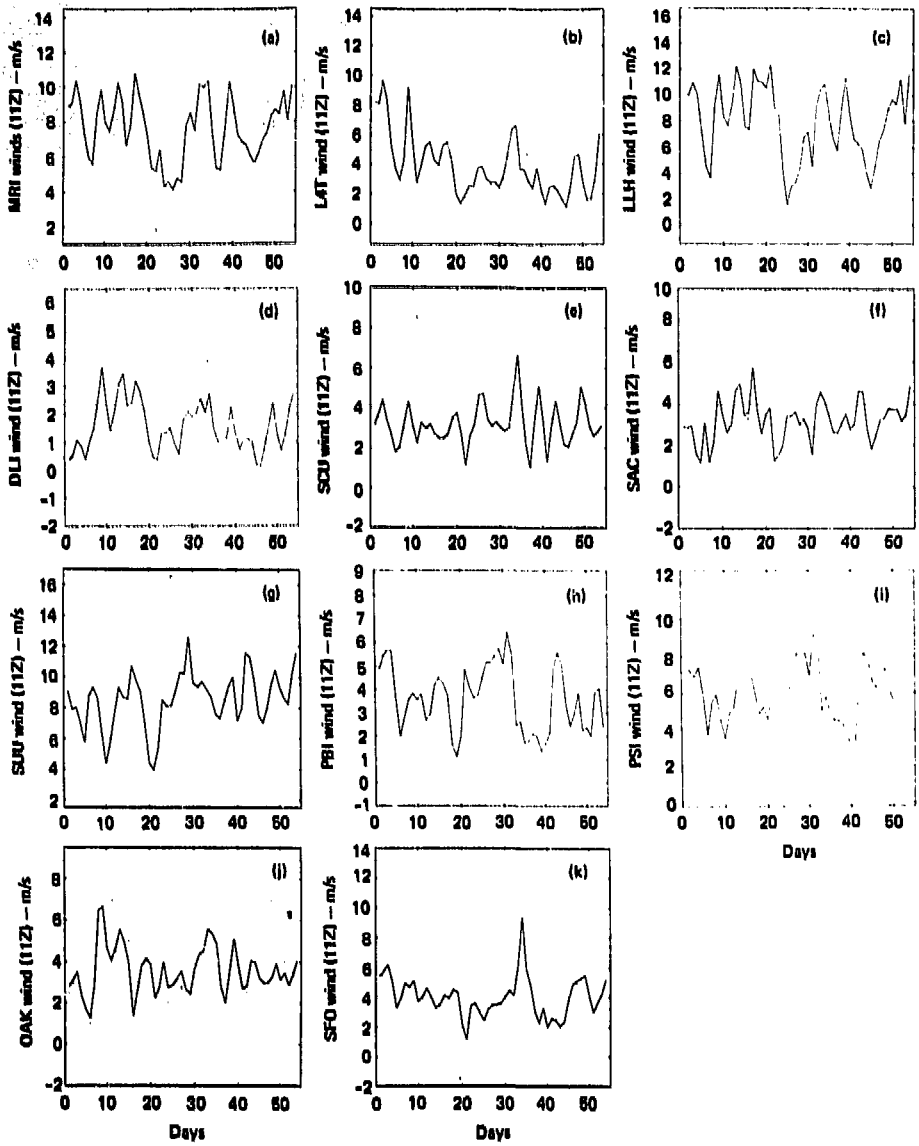

Fig. 10. Regional wind data at 1100 GMT or 11Z (0400 PDT).

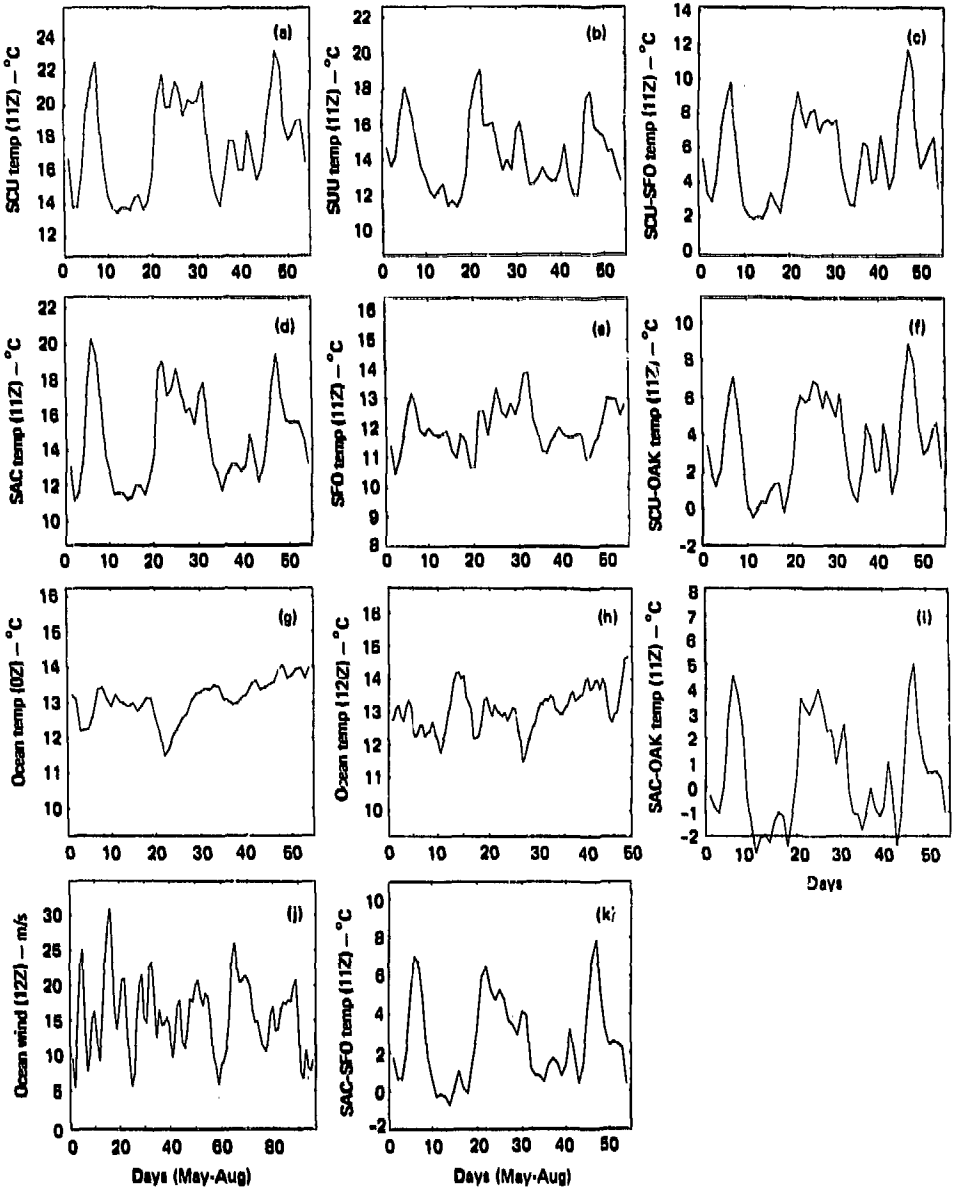

Fig. 11. Regional temperature and temperature-difference data with ocean parameter data at 11Z.

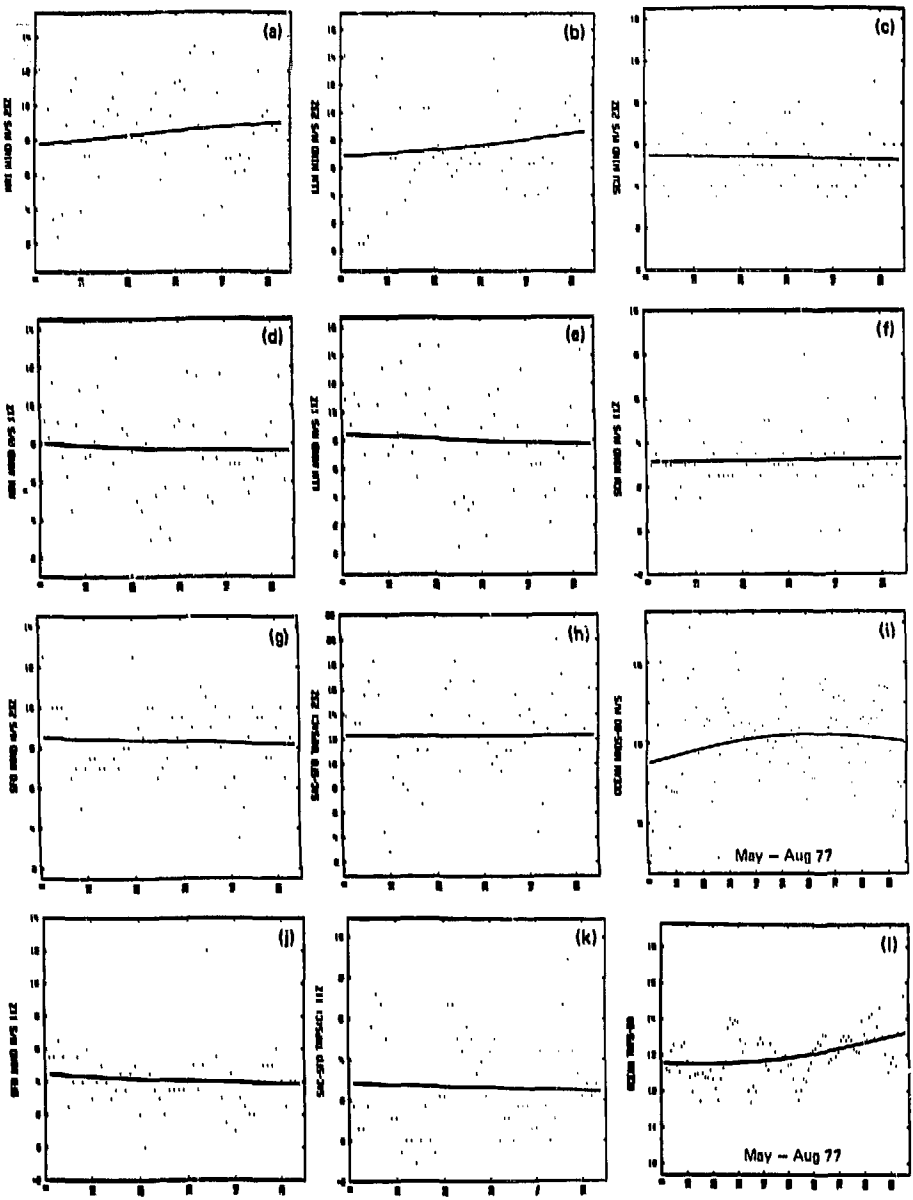

Fig. 12. Long-term trends of selected data from previous figures.

Table 3. Correlation matrix with regional wind speed, air temperature, and ocean parameters.

Y \ X	25X							11X						
	KTMP	SWND	KTMPB	SWNDB	MRI WND	LONG KTMP	LONG KTMPB	KTMP	SWND	KTMPB	SWNDB	MRI WND	LONG KTMP	LONG KTMPB
Wind speed: MRI	−0.30(3)	−0.47(2)	0.28(0)	−0.50(2)	1.0			0.53(2)	0.39(−4)	0.51(2)	0.41(−4)	1.0		
LHT	0.17(−1)	−0.32(2)	0.25(0)	0.40(−1)	0.73(0)			0.41(2)	0.24(1)	0.41(2)	0.27(0)	0.56(0)		
LLL	0.32(0)	−0.39(2)	0.44(0)	−0.44(2)	0.80(0)			0.49(2)	0.37(−4)	0.53(2)	0.41(0)	0.81(0)		
SCU	0.32(0)	−0.38(2)	0.28(0)	−0.41(2)	0.60(0)			0.11(1)	0.26(1)	0.20(1)	0.26(0)	0.37(0)		
OAK	−0.34(2)	−0.39(−4)	−0.32(2)	−0.40(−3)	−0.34(1)			0.29(2)	−0.51(4)	0.32(1)	−0.40(4)	0.43(0)		
SFO	−0.19(0)	0.26(−4)	−0.29(0)	0.35(1)	0.32(2)			0.24(1)	−0.39(4)	0.32(1)	−0.37(4)	0.35(0)		
SUU	−0.24(3)	−0.37(2)	−0.27(3)	−0.38(2)	0.63(0)			0.32(−1)	−0.25(3)	0.32(−1)	−0.26(2)	0.27(−1)		
SAC	0.09(3)	−0.36(2)	0.20(0)	−0.36(3)	0.60(0)			0.25(2)	−0.20(3)	0.33(2)	−0.23(3)	0.52(0)		
DLI					0.50(0)							0.56(0)		
PDI					0.51(0)							−0.22(1)		
PSI					0.39(0)							−0.28(1)		
Air temperature: SCU	−0.51(3)	0.43(3)	−0.64(1)	0.44(3)	−0.45(1)			−0.42(2)	−0.29(1)	−0.48(2)	−0.33(1)	−0.48(0)		
OAK	−0.39(0)	0.37(2)	−0.50(0)	0.43(2)	−0.45(0)			−0.18(2)	−0.29(2)	−0.19(2)	−0.28(0)	−0.14(0)		
SFO	−0.42(0)	0.47(2)	−0.49(0)	0.45(2)	−0.40(0)			0.26(−2)	−0.33(3)	−0.26(1)	−0.31(0)	−0.14(1)		
SUU	−0.45(1)	0.37(3)	−0.56(1)	0.44(3)	−0.59(0)			−0.33(0)	−0.12(0)	−0.31(0)	−0.14(0)	−0.33(0)		
SAC	−0.51(1)	0.41(3)	−0.64(1)	0.45(3)	−0.31(0)			−0.41(2)	−0.32(1)	−0.45(2)	−0.32(1)	−0.47(0)		
ΔSCU-OAK	−0.49(2)	0.36(5)	−0.61(2)	0.37(3)	−0.43(1)			−0.43(2)	−0.30(−3)	−0.50(2)	−0.30(1)	−0.52(0)		
ΔSCU-SFO	−0.39(2)	0.37(3)	−0.53(2)	0.41(3)	−0.39(1)			−0.42(2)	−0.29(−3)	−0.47(2)	−0.30(1)	−0.54(0)		
ΔSAC-OAK	−0.45(2)	0.31(5)	−0.58(2)	0.37(3)	−0.42(1)			−0.42(2)	−0.30(−5)	−0.46(2)	−0.30(−1)	−0.50(0)		
ΔSAC-SFO	−0.36(2)	0.35(5)	−0.50(2)	0.41(3)	−0.39(1)			−0.42(2)	−0.31(−5)	−0.43(2)	−0.33(−5)	−0.54(0)		
Ocean wind speeds: SWND					−0.47(−2)	0.36(6)					0.99(0)		0.38(6)	
SWND (⊥)	0.16(1)	0.99(0)			−0.47(−2)	0.36(6)		0.38(5)	0.94(0)			0.37(4)	38.(6)	
SWND (Short)	0.16(5)				−0.47(−2)			0.36(5)				0.39(4)		
SWND (⊥)	0.42(2)	−0.36(3)	0.36(2)	−0.42(2)	0.23(3)			0.35(1)	−0.36(3)	0.25(1)	−0.33(3)	0.29(0)		
SWNDB					−0.50(−2)		0.32(5)							0.35(6)
SWNDB (⊥)			0.37(5)	0.99(0)	−0.50(−2)		0.32(5)			0.47(5)	0.95(0)	0.39(4)		0.36(6)
SWNDB (Short)			0.39(5)		−0.50(−2)					0.47(5)		0.41(4)		
SWNDB (⊥)					0.28(−6)							0.29(−5)		

MRI = Patterson Pass
LHT = L.L.L. Tower 40 m
LLL = Site 300
SCU = Stockton
OAK = Oakland
SFO = San Francisco Airport
SUU = Travis AFB
SAC = Sacramento
DLI = Livermore (BAAPCD)
PDI = Bethel Island
PSI = Sherman Island

SWND = Ocean winds off San Francisco
SWND (⊥) = Wind component parallel to coast
SWND (⊥) = Wind component perpendicular to coast
SWNDB = Ocean winds off Monterey
SWND (Short) = Data period the same as that for land stations June and July (55 data pts)
SWND (Long) = May, June, July and August data (94 data pts)
STMP = Ocean temperatures at surface off San Francisco

Δ = Temperature differences
( ) = Time lag in days
+ ⇒ X leads Y
− ⇒ X lags Y

however, a new approach, called maximum entropy spectral analysis, has been developed for sparse data conditions.[13]

The basic idea of the maximum entropy method (MEM) is the minimal assumption about the unknown values of a stochastic process to fit filters (whitening) to obtain the reciprocal of the squared magnitude of the Fourier-transformed filter coefficients. Earlier methods artificially extend the data, assuming a zero or periodic signal with specified windows. The computer code developed by Strand uses a tapered entropy method (TEM), which fits a filter by optimal extension of the covariances to keep the covariant determinant properly bounded (i.e., positive definite).

Figures 13 and 14 show the results of the TEM spectral analysis with a matrix dimensionality of nine for regional winds at 2300 and 1100 GMT (see Fig. 2), regional air temperatures at 2300 GMT, and sea-surface temperatures and wind speeds at 0000 GMT and 1200 GMT off the coast of Monterey (Fig. 13). The spectra in Fig. 13 show large differences at frequencies above once per 4 days; however, at frequencies between once per 16 days and once per 4 days, a double-peak feature is characteristic. One peak occurs close to the once per 5-day peak found earlier in the 30-min-averaged data and the other peak ranges between once per 12 days and once per 16 days. This second peak is not observed at the Livermore tower (L4T) at night, possibly because it is the only one of the three stations below the nocturnal inversion at 1100 GMT. The air temperatures and ocean parameters in Fig. 14 also show this double maxima feature, but with less energy in the higher frequency peak. This spectral information, combined with the correlation matrix, provides a tool for the characterization of the mechanisms of the summer sea-breeze phenomenon.

APPLICATION TO MODEL VALIDATION

These data serve not only as a tool for understanding regional wind and temperature phenomena, but also as a data base to validate numerical wind-field models. Simultaneous data from 38 of the stations listed in Table 2 were passed through a multiple linear-regression analysis, with the wind speeds at Patterson Pass as the dependent variable. This was done assuming varying F-test criteria. The statistical F-test is the mean square due to regression divided by the mean square due to residual variation; it serves as a criterion for accepting data from another independent variable by making a statistically significant contribution to explaining the variance of the dependent variable.[14]

Table 4 shows the stations chosen under different F-test criteria and their distances from Patterson Pass. The stations chosen were not necessarily the stations closest to Patterson Pass or the ones that correlated best. Closer examination of the stations selected shows that they were chosen at locations sensitive to the many different wind-flow patterns characteristic of the greater Bay Area and the Central Valley. Figure 15 summarizes the results of the study shown in Table 4 and plots the number of stations chosen under the various F-tests versus the percent of the variance explained.

The graph of Fig. 15 serves two purposes. First, the sudden slope change, at approximately eight stations with 90% of the variance explained, implies that eight properly placed stations in the region could characterize the wind field in the region of complex terrain downwind of LLL (Patterson Pass) almost as well as many more stations in similar locations. More stations in the complex terrain region would be helpful because the only complex terrain measurements included in the data set were at Patterson Pass (the dependent variable) and the station at Site 300. Figure 15 includes a data point obtained by using only data from airport wind stations normally available for fast response to the Atmospheric Release Advisory Capability (ARAC) network. ARAC assesses in real time the downwind transport and diffusion of atmospheric releases at LLL.[15] Figure 15 shows that many more airport stations are required to explain the same amount of variance in the data at Patterson Pass as found with the regression-selected stations. A second conclusion from the results shown in Fig. 15 is that the stations selected can be used in a rational scheme for numerical model validation. By selective elimination of stations shown to be of value in predicting winds in complex terrain and comparison of the model results, models can be validated with some quantification of the importance of the station eliminated. The results of this kind of model-validation study will be discussed in a later report.

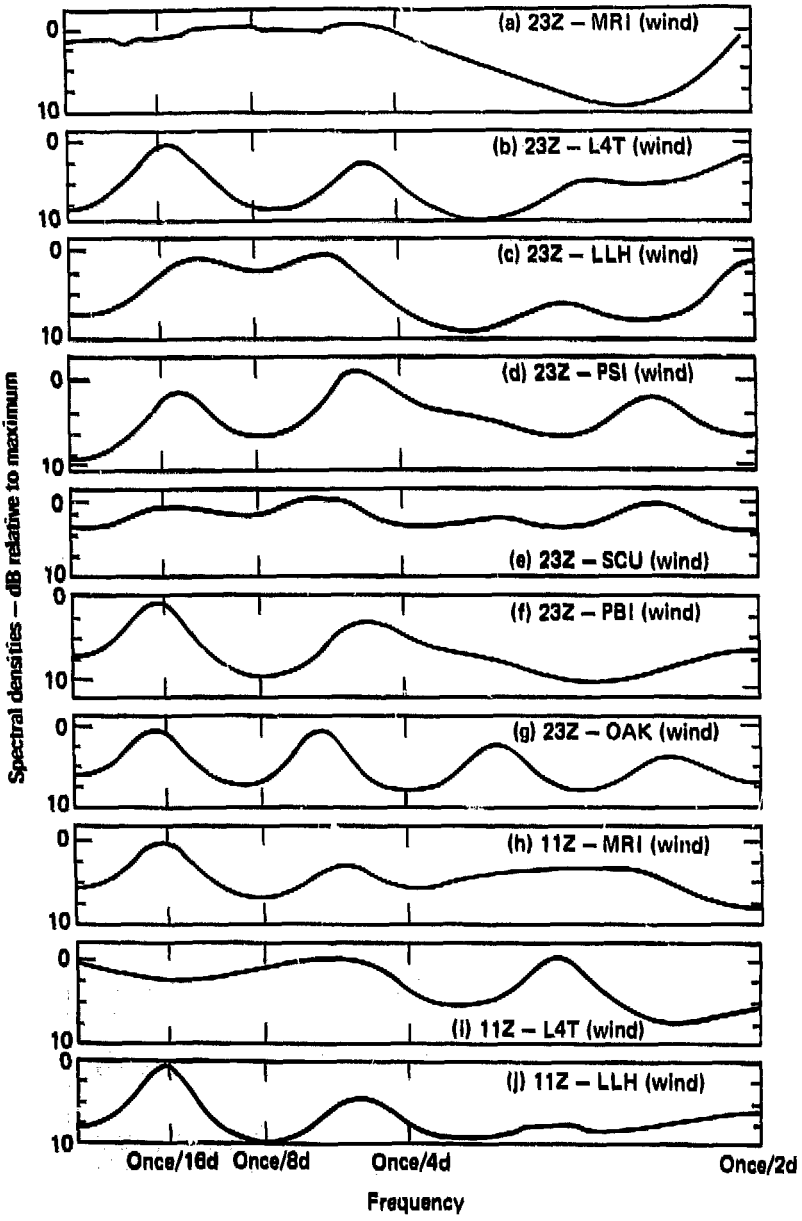

Fig. 13. Maximum entropy power spectra of regional wind speeds at 2300 and 1100 GMT.

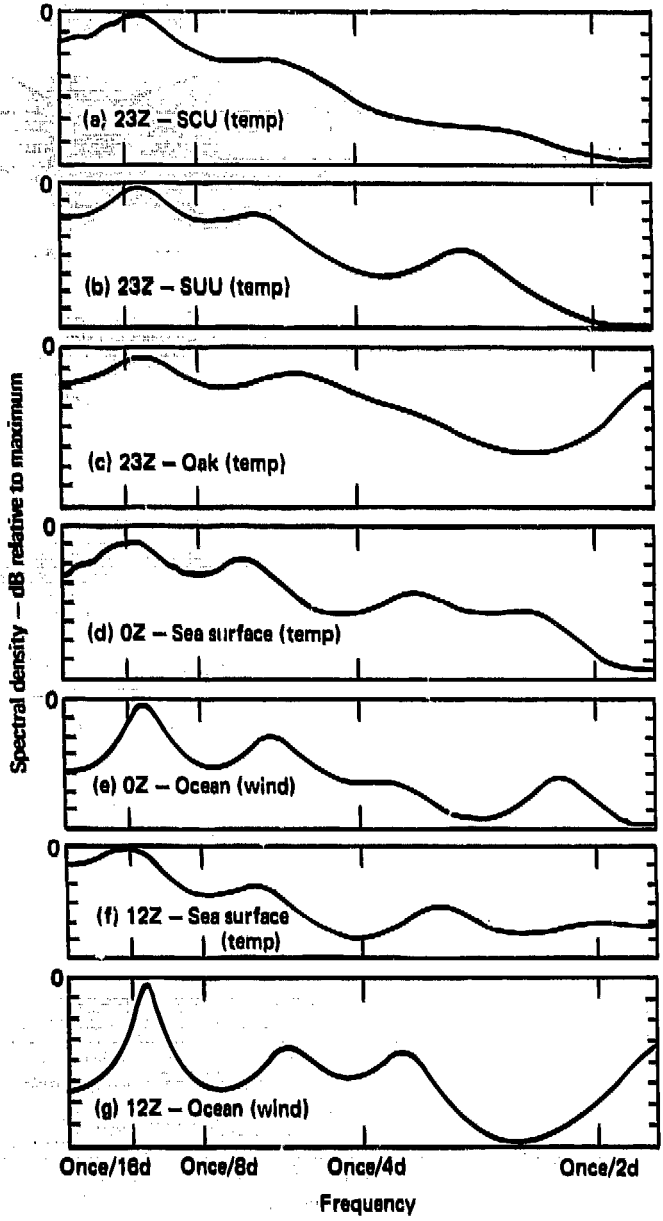

Fig. 14. Maximum entropy power spectra of regional temperatures and ocean parameters at 2300, 0000, and 1200 GMT.

Table 4. Stations selected from multiple linear regression analysis with Patterson Pass wind speeds as the dependent variable with F-test criteria (Yes → passes test).

Station	Distance from Patterson Pass, km	F-test 0.5	0.4	0.3	0.2	0.1	0.05	0.01
1. L4T (LLL Tower)	7.5	Yes	Yes	Yes	Yes	Yes	No	No
2. LLH (Site 300)	9.6	Yes	Yes	Yes	Yes	Yes	Yes	Yes
3. DLI (BAAPCD Livermore)	13.0	Yes	No	No	No	No	No	No
4. PBI (Bethal Island)	37.9	Yes	Yes	Yes	Yes	Yes	Yes	No
5. PSI (Sherman Island)	40.9	Yes	Yes	Yes	No	No	No	No
6. DCO (Concord)	45.3	Yes	Yes	No	No	No	No	No
7. NUQ (Moffett Field)	47.6	Yes	Yes	Yes	No	No	No	No
8. OAK (Oakland)	51.0	Yes	Yes	Yes	No	No	No	No
9. DRC (Redwood City)	55.5	Yes	No	No	No	No	No	No
10. DBE (Benicia)	62.1	Yes	Yes	Yes	Yes	Yes	Yes	No
11. CRT (Crockett)	64.1	Yes	Yes	Yes	Yes	Yes	No	No
12. CBM (Berkeley Marina)	64.4	Yes	Yes	Yes	Yes	Yes	N	No
13. DRM (Richmond)	70.9	Yes	Yes	Yes	Yes	No	No	No
14. DGL (Gilroy)	74.5	Yes	Yes	Yes	Yes	No	No	No
15. CMD (Menlo Park)	75.3	Yes	No	No	No	No	No	No
16. DSR (San Rafael)	85.0	Yes	No	No	No	No	No	No
17. EGL (Moss Landing)	97.8	Yes	Yes	Yes	No	No	No	No
18. MCC (McClellan AFB)	110.9	Yes	Yes	Yes	Yes	Yes	Yes	Yes
19. SNS (Salinas)	113.0	Yes	Yes	No	No	No	No	No
20. DSA (Santa Rosa)	127.4	Yes	Yes	Yes	Yes	Yes	Yes	No

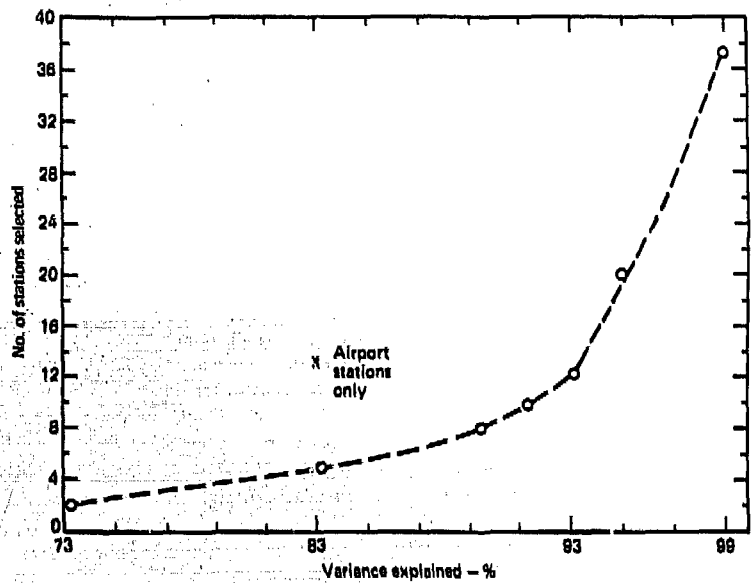

Fig. 15. Plot of the number of stations selected from 38 stations in the region, based on multiple linear regression with Patterson Pass wind speeds as the dependent variable and varying F-tests from 0.01 to 0.5 vs the resultant percent of variance explained.

CONCLUSIONS

The results described in this report can be separated into two categories. The first shows how statistical analysis of the data base can be applied to determine the summer sea-breeze flow patterns in the region; the second category of results shows how the data base can be applied to numerical wind-field model validation in complex terrain. The results listed below are significant in understanding the regional wind patterns during summer sea-breeze conditions:

1. Power spectral analysis of 15-min average wind data over 55 days in June and July 1977 at locations in and around a windy area of complex terrain downwind of LLL (Patterson Pass) showed strong spectral peaks once each day and once every five days.

2. Maximum entropy spectral analysis of daily data at 2300 GMT and 1100 GMT (typical times of maximum and minimum in sea-breeze intensity) at these locations and others revealed an even longer-term cycle ranging between once per 12 and 16 days.

3. Cycles of 5 and 12 days were also observed in sea-surface temperatures and ocean winds.

4. A weak correlation exists between the ocean parameters and regional winds.

5. A stronger correlation exists between the ocean parameters and regional air temperatures.

6. The sign of the correlation between regional air temperatures and sea wind reversed from positive during the day to negative at night.

7. A time lag of 1-3 days was noted between the ocean parameters and Central Valley air temperatures.

The conclusions listed below were derived from this data base which relate to numerical model validation in complex terrain.

1. Despite the high correlation coefficient (0.91) between space-averaged wind data from optical anemometers and wind data at one end of the path from a cup anemometer, these data often show differences of many metres per second, implying a single wind station cannot satisfactorily represent 30-min average winds over one kilometre in complex terrain.

2. These differences are lower for data of a longer time period.

3. Multiple linear regression is a successful technique for selecting stations that contribute most to the explanation of wind variations at the complex terrain location (Patterson Pass).

4. Multiple linear regression eliminates redundant and random data from consideration for model validation.

5. Multiple linear regression was successfully applied to determine the number of stations needed to characterize the wind flow over the region.

6. Multiple linear regression provides a rational selection criterion for data comparisons for numerical wind-model validation.

ACKNOWLEDGMENTS

The authors would like to thank M. Dickerson and J. Knox for their support with this project; P. Weidhaas and J. Huebel for their help with the multiple linear regression statistics; L. Lomonaco for data location help; H. Ellsaesser for advice; V. Arganbright for Site 300 data; G. Ochs, from NOAA/WPL, for advice and the loan of the white-light optical anemometer; P. Russell, from SRI, for the loan of an acoustic sounder; J. Pryshepa and R. Littlefield, from Cal Trans, for wind data; M. Mooney and R. Swanson, from PG&E, also for wind data; Lt. Commander Loveless, from the Fleet Numerical Weather Service, for the ocean data; J. Sandberg and T. McEwen, from the Bay Area Pollution Control District, for their data support; L. Gates for supervising the data reduction; and a special thanks to R. Vierra and E. Mulqueeney who permitted us to use their ranch land for our study, to C. Haakenstad who helped make the property arrangements, and to W. Stutler who built the instrument shelters.

REFERENCES

1. C.S. Sherman, *MATHEW: A Mass-Consistent Wind Field Model*, Lawrence Livermore Laboratory, Livermore, Calif., Rept. UCRL-52479 (1978).
2. R.S. Lawrence, G.R. Ochs and S.F. Clifford, "Use of Scintillations to Measure Average Wind Across a Light Beam," *Applied Optics* 11(2) (1972).
3. G.R. Ochs, S.F. Clifford and T. Wang, "Laser Wind Sensing, the Effects of Saturation of Scintillation," *Applied Optics* 15(2) (1976).
4. P.B. Archibald and J.B. Knox, *An Analysis of the Winds of Site 300 as a Source of Power*, Lawrence Livermore Laboratory, Livermore, Calif., Rept. UCRL-51469 (1977).
5. M.A. Fosberg and M.J. Schroeder, "Marine Air Penetration in Central California," *J. of Appl. Meteorol.* 5 (1966).
6. S.J. Savage, "Summertime Marine Air Penetrations to the City of Sacramento," Master's thesis, San Jose State University, San Jose, California (1967).
7. R.A. Anthes, "The Height of the Planetary Boundary Layer and the Production of Circulation in a Sea Breeze Model," *J. Atmos. Sci.*, 35(7) (1978).
8. J.D. Hawkins, "A Study of the Mesoscale Wind Circulation in a Land-Sea Breeze Regime," *Bull. Amer. Met. Soc.*, 58(12) (1977).
9. W.M. Porch, "Applications of Optical Anemometry," *Technical Digest of Topical Meeting on Meteorological Optics*, Keystone, Colorado (Aug. 1978).
10. M.J. Blanchet, R.E. Hodgen and H.J. Sollod, *Solar Radiation in Pacific Gas and Electric Company's Service Area*, Pacific Gas and Electric Company, San Francisco, California (June 1976).
11. A.S. Högstrom and U. Högstrom, "Spectral Gap in Surface-Layer Measurements," *J. of Atmos. Sci.*, 32 (1975).
12. R. Spirtas and H.J. Levin, "Patterns and Trends in Levels of Suspended Particulate Matter," *J. of Air Pollution Cntrl. Assoc.*, 2(6) (1971).
13. O.N. Strand, *A Computer Program for the Calculation and Analysis of Maximum Entropy Spectral Estimates*, National Oceanic and Atmospheric Administrations, Boulder, Colorado, Wave Propagation Laboratory Report (1975).
14. N. Draper and H. Smith, *Applied Regression Analysis*, Wiley and Sons, New York (1966).
15. M.H. Dickerson and R.C. Orphan, "Atmospheric Release Advisory Capability," *Nuclear Safety*, 17(3) (1976).

C.H.